ELSEVIER

Physica C 249 (1995) 53–68

PHYSICA C

Critical-current anisotropy, intergranular coupling, and effective pinning energy in $Bi_2Sr_2CaCu_2O_{8+\delta}$ single crystals and Ag sheathed $(Bi, Pb)_2Sr_2Ca_2Cu_3O_{10+\delta}$ tapes

P.J. Kung [a,*,1], M.E. McHenry [b,2], M.P. Maley [b], P.H. Kes [c], D.E. Laughlin [d], W.W. Mullins [d]

[a] *Biophysics Group P-6 and Superconductivity Technology Center, MS M715, Los Alamos National Laboratory, Los Alamos, NM 87545, USA*

[b] *Superconductivity Technology Center, MS K763, Los Alamos National Laboratory, Los Alamos, NM 87545, USA*

[c] *Kamerlingh Onnes Laboratory, Leiden University, PO Box 9506, 2300 RA Leiden, The Netherlands*

[d] *Department of Materials Science and Engineering, Carnegie Mellon University, Pittsburgh, PA 15213, USA*

Received 30 June 1994; revised manuscript received 19 April 1995

Abstract

$Bi_2Sr_2CaCu_2O_{8+\delta}$(Bi-2212) single crystals and Ag sheathed $(Bi,Pb)_2Sr_2Ca_2Cu_3O_{10+\delta}$(Bi-2223) tapes have been characterized by magnetometry and electron microscopy. Dislocations on the (001) planes appear to be the main defect observed in these samples and are considered to be important for flux pinning. Their distribution is more homogeneous in the Bi-2223 tape as a result of thermomechanical processing. In Bi-2212 single crystals, the measurement of magnetic hysteresis reveals a strong anisotropy in the magnetization critical current density (J_{cm}). For the two cases $H \parallel c$ and $H \perp c$, the measurable Lorentz forces (F_L) that limit J_c are found to be perpendicular to the c-axis; one causing vortices to hop in the *ab* plane and the other to slide along the *ab* plane. In contrast to this, we have probed the relative strength ratio of the intrinsic pinning to the extrinsic pinning in Bi-2223 tapes when we compare the results of $H \perp c$ with $H \parallel c$. No significant difference in J_{cm} is observed, but for the same average J value, the effective pinning energy (U_{eff}) calculated from the time derivative of the magnetization (M) for $H \perp c$ is two orders of magnitude higher than that for $H \parallel c$. For these two superconductors, their U_{eff}'s follow a power-law expression, $U_{eff}(J, T, H) = (U_i/H^n)[1 - (T/T_x)^2]^{1.5}(J_i/J)^{\mu}$, where U_i is the scale of activation energy, n is of the order of 1, T_x is related to the magnetic irreversibility temperature (T_{irr}), and both J_i and μ depend on the flux-bundle size and the value of J/J_c. A two-dimensional (2D) flux-line lattice (FLL) is clearly identified in the Bi-2212 single crystal; however, imperfect texturing in the Bi-2223 tape smears out to some extent the observed J dependence of U_{eff}. Consequently, a larger anisotropy in the normalized relaxation rate, $S = -\mathrm{d} \ln M/\mathrm{d} \ln t$, and much higher S values are observed in Bi-2212 than in Bi-2223.

1. Introduction

Energy dissipation due to the motion of vortices in the Bi based high-temperature superconductors

* Corresponding author.

[1] Current address: AFR, Inc., 87 Church Street, East Hartford, CT 06108, USA.

[2] Permanent address: Department of Materials Science and Engineering, Carnegie Mellon University, Pittsburgh, PA 15213-3890, USA.

SSDI 0921-4534(95)00281-2

($Bi_2Sr_2CaCu_2O_{8+\delta}$(Bi-2212) and $(Bi,Pb)_2Sr_2Ca_2Cu_3O_{10+\delta}$(Bi-2223)) is not only more severe but also involves new physical phenomena not observed in $YBa_2Cu_3O_7$ (Y-123). These differences can be attributed to the lack of appropriate pinning centers in the bulk of the materials and weak coupling between the CuO_2 superconducting planes in the Bi based superconductors. In Y-123, when $H \parallel c$, which is the direction with the most pronounced field dependence of J_c, twin planes and homogeneously distributed secondary-phase precipitates (e.g., Y_2BaCuO_5) are considered to be important pinning sites [1–3]. For Bi-2212 and Bi-2223, on the other hand, the pinning at high temperatures due to defects such as dislocations and stacking faults is not significant [4,5]. In contrast to a three-dimensional (3D) flux-line lattice (FLL) in Y-123, the much larger anisotropy in the Bi-2212 compound results in a two-dimensional (2D) Josephson coupled system as widely proposed. The 2D characteristic of $J_c(H, \theta)$, where θ is the angle between the magnetic field H and the normal to the *ab* plane, has been revealed from the measurements of critical current anisotropy performed on epitaxial Bi-2212 thin films and on well aligned Ag sheathed Bi-2223 tapes [6,7].

A picture of 2D vortex pancakes has been suggested to describe the Bi based superconductors, in which dissipation in the system is predominantly related to the magnetic-field component perpendicular to the CuO_2 planes [8]. As such, intralayer pinning and vortex interaction play a significant role in determining the resulting flux-creep behavior. When $H \perp c$, vortex cores are favored energetically to stay within the insulating layers sandwiched between the CuO_2 planes. The insulating layers thus can be viewed as intrinsic pinning sites [9]. These arguments have important implications for the determination of the effective pinning energy $U_{eff}(J, T, H)$ including

(1) significant differences in the equilibrium H–T phase diagram in the 2D system as opposed to the 3D system, and

(2) if the sample is completely textured (in terms of perfect local grain alignment) and only pinning by background mechanisms is present, a comparison of $U_{eff}(H \parallel c)$ with U_{eff} $(H \perp c)$ reflects the intrinsic flux-pinning anisotropy of the material.

In spite of their significant anisotropy and weak interlayer coupling, the Bi based superconductors do have certain advantages over those with Y-123. These include a higher T_c and their plate-like morphologies. The last factor aids in obtaining a better grain alignment by the thermomechanical deformation process in the Bi based compounds. Therefore, for years significant effort has been made to fabricate Ag sheathed Bi based superconducting tapes using the oxide-powder-in-tube (OPIT) technique [10–12]. It turns out that highly textured and dense bulk conductors with the *c*-axes of the individual crystals parallel to the tape thickness can be obtained. As suggested by the ''brick-wall'' model [13], such textured structures and plate-like morphologies developed in the Bi based compounds provide enough contact areas between individual grains so that current can be effectively shunted via large-area Josephson junctions perpendicular to the *c*-axis (i.e., current flowing across (001) twist boundaries) when weak links (e.g., (001) tilt boundaries) are presented in the direct path of the current. In other words, the superconducting properties of the layers resided at (001) twist boundaries, for instance, the Bi-2212 phase in Bi-2223 tapes [14], determine the overall observed T_c and transport critical current density, J_{ct}, of the tapes.

Recently, some experimental observations have shown to disagree with the ''brick-wall'' model. The ''railway-switch'' model [15] proposed that J_{ct} in Bi-2223 tapes is controlled by small-angle *c*-axis grain boundaries. Due to a high degree of their crystallinity, these boundaries effectively link neighboring grains and allow a supercurrent to pass without flowing perpendicularly to the CuO_2 planes. In the experiments carried out by Cho et al. [16], current was also found to flow predominantly along the crystallographic *ab* planes in the J_{ct} measurements with a current applied parallel to the rolled tape normal. The anisotropy of the resistivity was obtained to be small, in the range of 4–10 among the five rolled tapes with an average *ab* plane misalignment of about 8–10° with respect to the tape surface. These results imply that the transport flow pattern may not be simple as suggested by the ''brick-wall'' model. It likely depends upon local intergrain alignment and the stoichiometry of the intergranular regions.

Investigation of microstructure, magnetic hystere-

sis and relaxation can provide insights into the intergranular coupling and intragranular flux-pinning characteristics in the Ag sheathed Bi-2223 tapes. This would be impossible to use to figure out exactly on a microscopic level how currents flow inside a tape (e.g., brick-wall versus railway-switch), but it will give information on the relationship among texturing, flux pinning, dimensionality, and anisotropy that can be further correlated with observed J_c and T_c results. Such approaches are of great importance for applications of bulk superconductors. $Bi_2Sr_2CaCu_2O_{8+\delta}$ single crystals and silver-sheathed $(Bi,Pb)_2Sr_2Ca_2Cu_3O_{10+\delta}$ superconducting tapes are, therefore, characterized by magnetometry and electron microscopy. We measured magnetic hysteresis and relaxation for two cases: magnetic field parallel to the c-axis (hereafter, $H \parallel c$) and perpendicular to the c-axis ($H \perp c$). Because
(1) intergrowths often occur in the Bi based system and
(2) perfect c-axis texturing has not been obtained in our Ag sheathed tapes, we must study high-quality single crystals in order to clearly distinguish the pinning behavior with $H \parallel c$ from that with $H \perp c$. Nevertheless, to date, phase-pure Bi-2223 single crystals have not yet been successfully synthesized. Therefore, Bi-2212 single crystals are chosen and studied for comparison. Although different T_c's are observed between Bi-2212 and Bi-2223, they both have similar anisotropic layered crystal structures. We have found that because of the aspect ratios of our Bi-2212 single crystals, the Lorentz force (F_L) that limits J_c is observed to be along the ab plane for both the case of $H \parallel c$ and of $H \perp c$ (which might have been misinterpreted by others). In the Ag sheathed tape, owing to a reduced anisotropy, we are able to probe the Lorentz forces that are parallel to the ab plane and the c-axis for $H \parallel c$ and $H \perp c$, respectively. The flux-creep characteristics of these two material systems can be well described in the framework of a power-law dependence of U_{eff} upon J.

2. Experimental

$Bi_2Sr_2CaCu_2O_{8+\delta}$ single crystals were grown by the traveling-solvent floating-zone technique [17]. The crystallinity of the single crystals was investigated by high-resolution transmission electron microscopy. $Bi_2Sr_2CuO_{6+\delta}$ intergrowth was found to occur in approximately 1 out of 500 CuO_2 double layers. For measurements, the average dimensions of the single crystals are of the order of $1.90 \times 1.85 \times 0.10$ mm^3. The Laue diffraction method and microstructural analysis indicate the c-axis is oriented parallel to the smallest dimension (0.1 mm) of the single crystal. This allows for an unambiguous comparison of the effective pinning energy $U_{eff}(J, T, H)$ in the ab plane and along the c-axis.

Ag sheathed $(Bi,Pb)_2Sr_2Ca_2Cu_3O_{10+\delta}$ tapes were fabricated by a standard oxide-powder-in-tube process. The nominal composition of the precursor powder was $Bi_{1.9}Pb_{0.3}Sr_2Ca_{2.2}Cu_3O_{10+\delta}$. The partially sintered precursor powder was loaded into a silver tube with an outer diameter of 6.35 mm and an inner diameter of 4.35 mm that was first cleaned and dried. This composite was then swaged, drawn, heat-treated, rolled, heat-treated, and pressed into a tape. A final heat treatment was applied to the tape. The overall cross-sectional area of the monofilament tape was 0.3×0.016 cm^2. The superconducting core was 0.24 cm wide and 100 μm thick, as determined from scanning electron micrographs. A piece of 2 cm in length was cut from the as-processed tapes for transport measurements. A 0.35 cm long piece was used for magnetization measurements and later sectioned to examine the intergranular coupling of the tape.

The surface morphologies of the crystals and tapes were observed using a scanning electron microscope (SEM; Series 4, CamScan). Interchange of the operating modes between secondary and backscattered electron images was sometimes used to clearly distinguish precipitates from the matrix phase of the sample. Transmission electron microscopy (TEM; CM30, Philips) was employed to study microstructure and crystallite orientation. Both images and electron diffraction patterns were recorded.

Superconducting transition temperatures T_c's (for the samples being cooled in zero field and in a field of 10 Oe), magnetic hysteresis (from 0 to 5 T at various temperatures) and relaxation (isothermal data points recorded for 3 h at various temperatures and magnetic fields) were measured by a superconducting quantum interference device (SQUID) magne-

tometer (MPMS, Quantum Design). A scan length of 3 cm was used in order to minimize the inhomogeneity of the magnetic field. This leads to field variation less than 0.05%. The differential sensitivity of the SQUID is about 10^{-8} emu and the temperature stability below 100 K is $\pm 0.5\%$. The transport critical current density, J_{ct}, is measured by a standard four-probe method, with a voltage criterion of 1 μV/cm. The voltage resolution from the measurement system is 10^{-9} V, and the stability of the temperature during the I–V measurement is about 0.05 K.

3. Results and discussion

3.1. Microstructural analysis of Bi-2212 single crystals

The as-grown Bi-2212 single crystals show a lamellar morphology with many microscopic steps on the *ab* planes. According to Laue X-ray diffraction analysis, the *c*-axis was found to be perpendicular to the growth direction (i.e., the *ab* plane). Superlattice structures were observed by TEM in the crystals. The wavevectors of the modulation are $q = 0.21b^*$ and $q = 0.42b^*$, as often seen in the Bi-2212 superconductor [18,19]. The occurrence of a superstructure, as previously suggested, is possibly caused by the ordering of cation and/or oxygen defects [20,21]. It is worthy to mention here that the pinning force by oxygen vacancies in the CuO_2 double layers has been computed for Bi-2212, and these point defects are suggested to pin vortices effectively at large fields [22]. Although we have not made the effort to study the density and distribution of oxygen vacancies in our crystals, we are not ruling out the possibility of their contributions to vortex pinning.

In the Bi based superconductors, because of the micaceous layered structure and very weak bonding between the BiO layers, dislocations usually occur in the basal (001) plane [23]. These dislocations can either accommodate a local stress or form as defects due to the crystal growing in preferential directions. In order to have a minimized energy, the interaction between partial dislocations may easily occur to form dislocation networks [24]. Fig. 1 shows the TEM image and diffraction pattern of a dislocation network. Two different types of modulations that we mentioned earlier occur here along the same direction (see Fig. 1(b)). From the image, two characteristic angles between any two kinked dislocations in the network can be clearly seen: 90° and 135°. This has been rationalized as a consequence of the perfect Burgers vector [100] dissociating into two orthogonal partials of $\frac{1}{2}[110]$ and $\frac{1}{2}[1\bar{1}0]$ in the *ab* plane [25]. In this work, we have not studied this feature in more

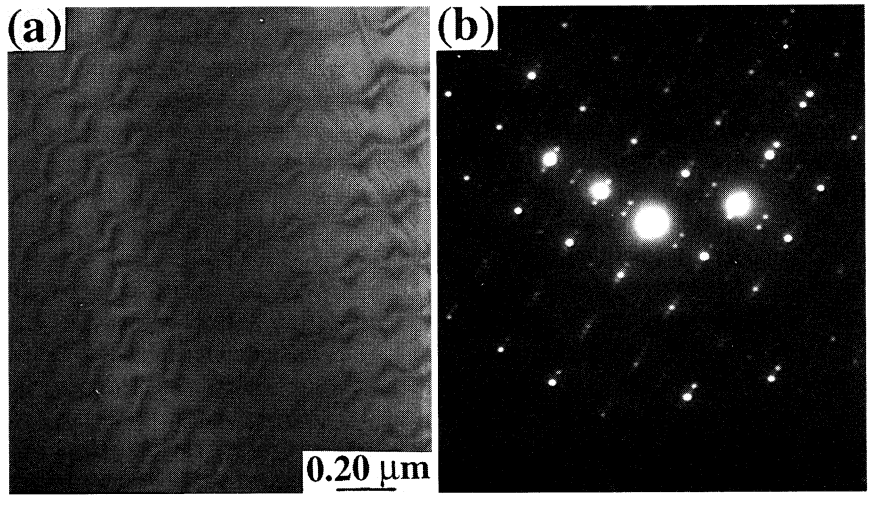

Fig. 1. (a) A TEM image of a dislocation network and (b) its corresponding [001] diffraction pattern with an overlay of two modulations of $q = 0.21b^*$ and $q = 0.42b^*$ observed from a Bi-2212 single crystal. The dislocation density is estimated to be of the order of 10^9 cm^{-2}.

detail because it is not our major concern. However, it can be understood as follows. Because the Bi based superconductors are easily cleaved along the basal *ab* plane, the two shortest lattice vectors in this plane, $\frac{1}{2}[110]$ and [100], are the most likely Burgers vectors for dislocations. When slip takes place, splitting of a perfect dislocation into partials is inevitable. Since the energy associated with a dislocation is proportional to the square of the magnitude of its Burgers vector, [100] is not energetically favorable and hence is liable to dissociate. As a result, Burgers vectors of $\frac{1}{2}\langle 110\rangle$ type turn out to be the most stable ones. An example analogous to this can be found in the slip of {111} planes in face-centered cubic crystals with the slip direction $\langle 110\rangle$. The dislocation density, as observed from the single crystal we studied, is estimated to be of the order of 10^9 cm^{-2}. The spacings between dislocation lines are not very uniform, varying from 20 to 150 nm. This order of magnitude is comparable to the lattice constant of the vortex in magnetic fields of 0.1–5 T. It suggests that these dislocations in the (001) plane, which are the main microstructural defects observed in our crystals, may be important for flux pinning.

3.2. Textured structure of Ag sheathed Bi-2223 tapes

To confirm the texture induced by cold work and heat treatment, the as-processed tapes were examined by X-ray diffractometry (XRD). Most of the XRD peaks can be indexed as the (00*l*) reflections of the Bi-2223 phase, which indicates the *c*-axes of individual grains to be perpendicular to the tape surface. The tape sample is relatively free of impurity phases (e.g., Ca_2PbO_4). In-plane misorientation of the (00*l*) textured grains still exists. Examination of the inside superconducting core shows a closely packed plate-like morphology. The degree of *ab* plane texturing can be improved as the number of cold rolling or pressing (for grain alignment) and sintering cycles (for grain growth) increases.

The microstructures of the tapes were also studied by TEM. The incommensurate modulation of the wavevector along the *b*-axis was estimated to be 0.208 ± 0.002. As mentioned earlier, deformation-induced defects are easily introduced into Bi based superconductors because of their mica-like layered structure. For instance, a set of nearly parallel dislocations with spacing 50 nm is found evidence for in Fig. 2(a). In certain regions, these dislocations interact with each other, which probably results from recovery during final heat treatment. Besides dislocations, cleavage, wrinkling, and sliding between BiO layers can result in a moiré pattern (see Fig. 2(b)) if the condition for double diffraction is also satisfied. These moiré fringes are approximately spaced by about 66 Å. These microstructural defects, along with the low-angle (001) twist grain boundaries that were previously reported by Dou et al. [26], should provide, to some extent, a flux-pinning function and

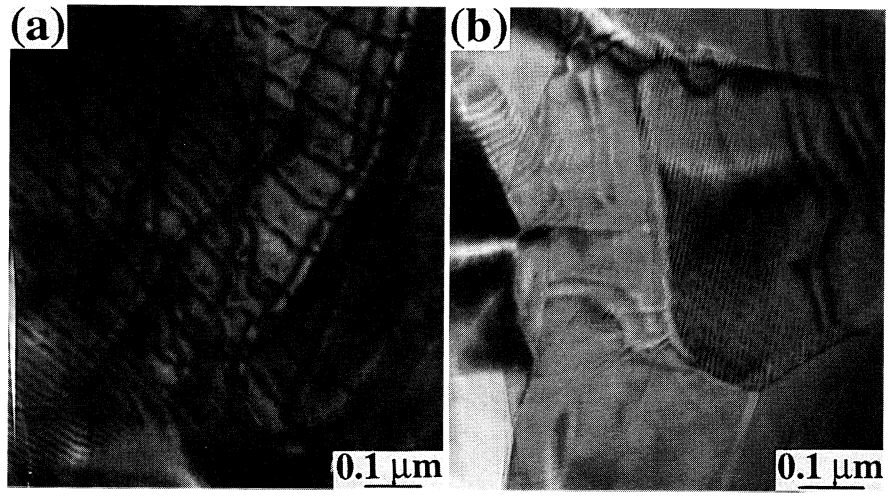

Fig. 2. (a) A set of nearly parallel dislocations and (b) a moiré pattern imaged from the Ag sheathed $(Bi,Pb)_2Sr_2Ca_2Cu_3O_{10+\delta}$ tape.

hence the improvement of $J_c(H)$ behavior in the Ag sheathed Bi-2223 tapes.

3.3. J_{cm} and its anisotropy in Bi-2212 single crystals

The Bi-2212 single crystal exhibits $T_{c\,onset} = 85$ K in the magnetic field of 10 Oe. Magnetic-hysteresis loops (see Fig. 3) were measured for both $H \parallel c$ and $H \perp c$ up to 5 T after zero-field cooling the sample. Notice that, since we do not correct for the demagnetization effect, the shape of the hysteresis loops is affected to some extent in the low-field regime. As a matter of fact, such a correction also relies on the exact field and temperature dependence of critical current densities and determination of this relation is not straightforward. Nevertheless, both J_{cm}'s for

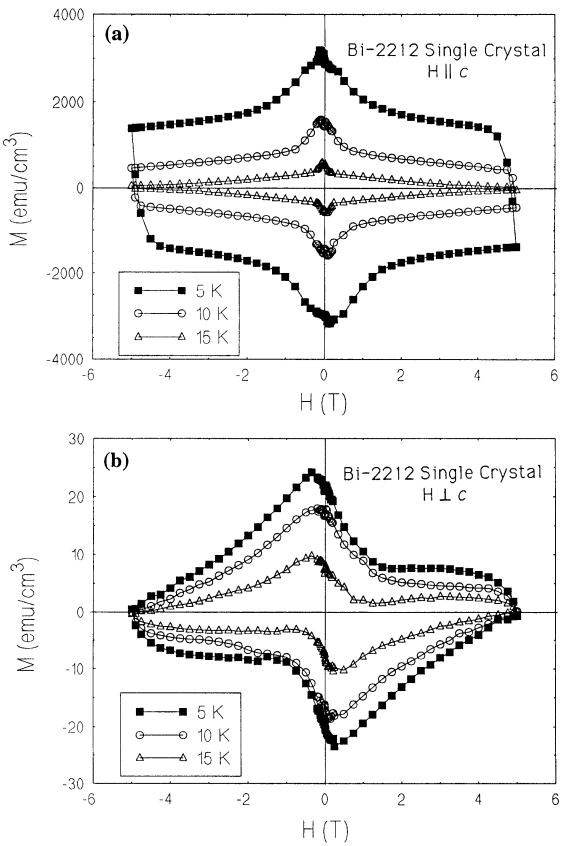

Fig. 3. Magnetization-hysteresis loops of the Bi-2212 single crystal for (a) $H \parallel c$ and (b) $H \perp c$.

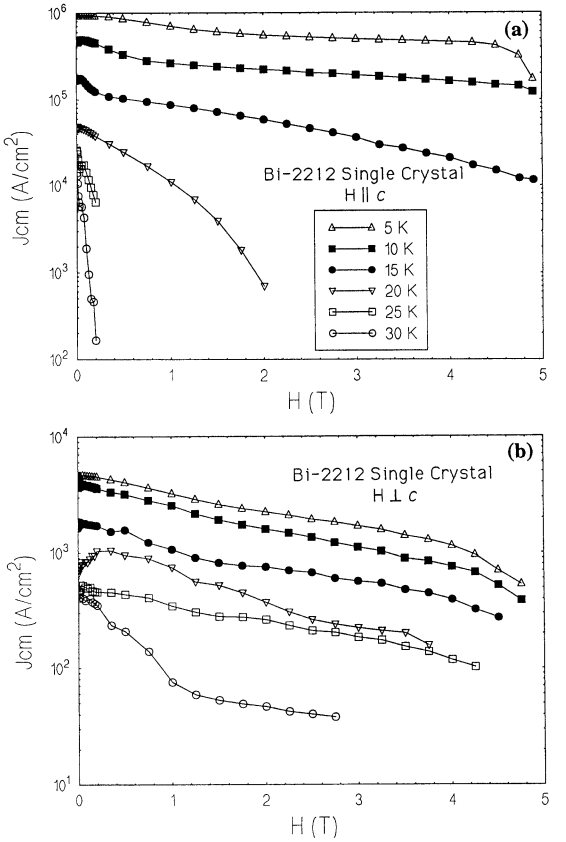

Fig. 4. Magnetic field dependence of J_{cm} in a Bi-2212 single crystal for (a) $H \parallel c$ and (b) $H \perp c$.

$H \parallel c$ and $H \perp c$ are derived from these $M(H)$ curves using the Bean model [27,28],

$$J_{cm} = \frac{20(M^- - M^+)}{a\left[1 - \left(\frac{a}{3b}\right)\right]} \quad (\text{for } H \parallel c), \tag{1}$$

$$J_{cm} = \frac{20(M^- - M^+)}{d} \quad (\text{for } H \perp c), \tag{2}$$

where M^+ and M^- are magnetization at increasing and decreasing applied fields, respectively; a and b ($b > a$) are the width and length of an orthorhombic cross-section, and d is the sample thickness along the direction of field penetration. As can be seen in Fig. 4, the magnitude of magnetization $\Delta M\ (\sim J) = M^- - M^+$ and the field dependence of J_{cm} in these two orientations are very different. Figs. 5(a) and (b) are drawn to explain this large anisotropy. In the

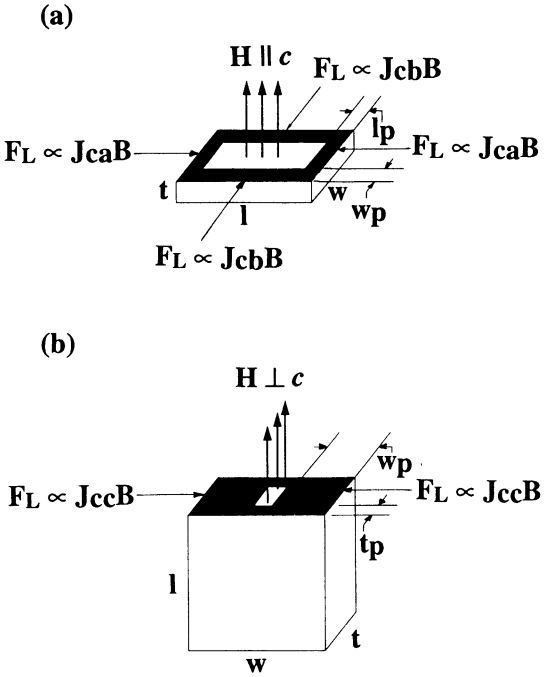

Fig. 5. Illustration of the current flow path, the flux penetration, and the direction of the Lorentz force F_L ($\propto J_c \times B$) in Bi-2212 single crystals for (a) $H \parallel c$ and (b) $H \perp c$. J_{ca}, J_{cb}, and J_{cc} are the critical current densities along the wl, and t direction, respectively. The shaded area represents the region penetrated by flux lines.

case of $H \perp c$, because of the large anisotropy in electrical conductivity of this compound [29], the conservation law of currents implies that $t_p \ll w_p$, where t_p and w_p are the respective depths of penetration of the flux profile along the directions of thickness (t) and width (w) of the crystal. Furthermore, our crystal has the aspect ratio of $w : t = 18.5 : 1$, and this leads to the expectation that $tJ_c(\parallel ab) \gg wJ_c(\parallel c)$. These results consequently suggest that flux penetration is predominantly along the width direction. Such a justification can also be examined by comparing the magnetization before and after cutting the crystal. Although we have not performed this kind of measurement, the cutting experiments done by Biggs et al. [30] in their single crystals with different aspect ratios ($w/t = 8$–23) confirm the above argument. When $H \parallel c$, on the other hand, the critical state is governed by J_c in the ab plane where the Lorentz force is also in the ab plane. This is because $J_c(\parallel a)$ and $J_c(\parallel b)$ are nearly of the same order of magnitude [29] and $l \approx w$. Flux lines then penetrate the crystal in a 2D fashion. In this regard, Eqs. (1) and (2) have to be employed for calculating $J_{cm}(H \parallel c)$ and $J_{cm}(H \parallel ab)$, respectively. In Fig. 4, at $T = 5$ K, in zero field, the corresponding J_{cm}'s are about 10^6 A/cm^2 and 5×10^3 A/cm^2 for $H \parallel c$ and $H \perp c$. The anisotropy ratio is about 200. This corroborates the expectations discussed above and previously established by Biggs' group [30].

The pinning mechanism responsible for $J_{cm}(H)$ can be understood with the aid of Fig. 5. In the case of $H \parallel c$, we have two components for the Lorentz forces: one along the length direction ($\parallel l$ direction in the ab plane) and the other parallel to the width direction ($\parallel w$ direction in the ab plane). These two forces are proportional to $J_{ca}B$ and $J_{cb}B$, respectively. When $H \perp c$, in principle, we should also consider two components: $J_{ca}B(\parallel t$ direction or c-axis) and $J_{cc}B(\parallel w$ direction or ab plane). Notice that, if the Lorentz force points in the thickness direction, which is parallel to the c-axis (or t direction), it basically balances with a pinning force due to the intrinsic pinning mechanism. A high effective pinning energy thus will be obtained; however, this is not probed in our experiments. Only the Lorentz force along the width direction was measurable in the case of $H \perp c$, and this force caused the vortices to slide along the ab plane. An anisotropy of the macroscopic pinning force density $F_p = J_c \times B$ versus H is shown in Fig. 6. As can be expected (by taking into account the values of l, w, and t), in the case of $H \parallel c$, although F_p's are ten times larger than those in $H \perp c$, the position of the F_p maximum for $H \parallel c$ actually shifts a larger amount towards the lower field with increasing temperature. This is probably due to a higher upper critical field in the ab plane than along the c-axis [31].

3.4. J_{ct}, J_{cm}, and examination of intergranular coupling in Bi-2223 tapes

The superconducting transition of the Bi-2223 tapes measured by magnetometry at a field of 10 Oe shows $T_{c\,onset} = 110$ K, and significant magnetic irreversibility is obtained as one compares the zero-field cooling (ZFC) and the field-cooling (FC) signals. Fig. 7 illustrates transport critical current densities,

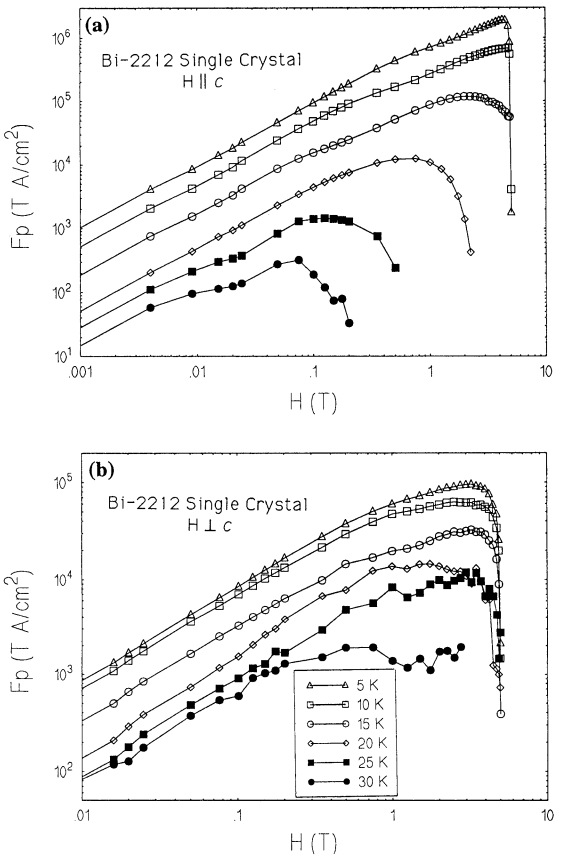

Fig. 6. Field dependence of the pinning force density F_p in a Bi-2212 single crystal for (a) $H \| c$ and (b) $H \perp c$.

J_{ct}, as a function of magnetic field over the temperature range of 20–75 K for the case of $H \| c$ in a Bi-2223 tape. As can be seen, a nearly exponential field dependence of J_{ct} at all temperatures is exhibited. This seems to be the typical behavior in the Bi based superconductors when a field component is parallel to the c-axis [15]. Although J_{ct}'s exceeding 10^4 A/cm^2 are observed at low temperatures, the dramatic drop of J_{ct} with magnetic field for $T > 35$ K at high fields is universal for this material [12,32]. This then restricts the applications of the tapes and also indicates that process-induced defects such as dislocation networks and oxygen vacancies have a limited ability to pin flux. In contrast to this, columnar defects introduced by heavy-ion irradiation recently have been shown to significantly enhance critical current densities at high temperatures and fields [33].

Results of the critical current density measured by a transport technique (J_{ct}) and by a magnetization method (J_{cm}) are very different. This is due to different experimental time constants as well as possibly different current-carrying length scales [32]. Therefore, when one measures J_{cm}, sectioning the tapes to determine the effective supercurrent-circulating dimensions is necessary. If no weak links are present, a critical-state scaling relation of the magnetization M with sample size d, $J_{cm} d \propto M$, should be observed. This means that the hysteresis loop of the cut sample is multiplied by a "scaling factor", which is determined from the reduction ratio of the sample dimensions after the sample is cut, and compared with that of the uncut sample. To perform this, the tapes were cut half along the direction parallel to the applied magnetic field for both $H \| c$ and $H \perp c$ measurements. Such a procedure and experimental results have been described in detail in a previous paper [34]. Some relevant arguments and observations are summarized as follows:

(1) If the scaling factor is progressively reduced at higher temperatures, it suggests that the granularity in the sample is induced by increasing temperature [12,35].

(2) Our data require larger scaling factors at higher temperatures. This can be understood as a result of a

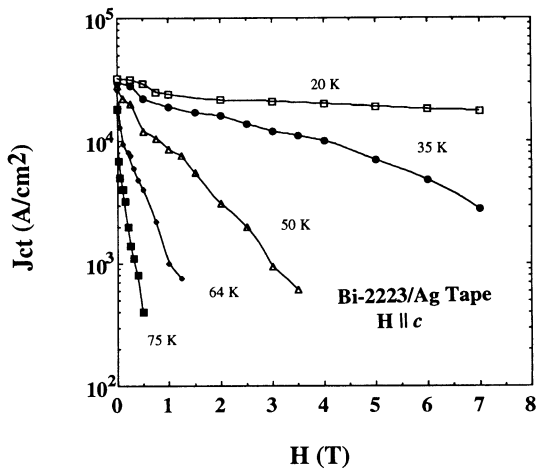

Fig. 7. Transport critical current densities for a Bi-2223 tape in $H \| c$ at various temperatures.

faster decay of the magnetization in the smaller sample. It is related directly to the fast relaxation of the Bi based superconductors and to an implicit scaling of the magnetic-diffusion equation with sample dimension.

We conclude from the cutting experiments that for $H \parallel c$, magnetization currents flow over a length scale equivalent to the sample size of our tapes (i.e., the same as Fig. 5(a)). However, in the case of $H \perp c$, the results show that neither the length nor width dimensions of the tapes follow the scaling relation of magnetization, indicating that the critical state is controlled by the thickness dimension. This implies that $\Delta M(=M^- - M^+) \propto J_{cb}t$ or $J_{ca}t$ and that the penetration of vortices is along the thickness direction. Note that this is the opposite conclusion from that reached for the Bi-2212 single crystal as described earlier (see Section 3.3). It also means that for $H \perp c$, $J_{ca}B$ or $J_{cb}B$ measured for the Bi-2223 tapes is probing the intrinsic pinning for vortex motion along the c-axis.

Fig. 8 shows the magnetic-hysteresis loops for three different temperatures and a comparison of these loops between $H \parallel c$ and $H \perp c$. From the hysteretic response, magnetization currents can be derived from Eqs. (1) and (2) (notice that instead of $d = w$ in the case of Bi-2212 single crystals, $d = t$ is used here) and depicted in Fig. 9. Higher J_{cm} values are observed for $H \perp c$ than those for $H \parallel c$, which was also previously reported by Kase's group [36]. In addition, an increasing anisotropy in J_{cm} with increasing temperatures is present here, and J_{cm} for $H \parallel c$ has a stronger field dependence, which is also revealed from the curves of the maxima of pinning force density versus magnetic field as plotted in Fig. 10. These observations imply the important role, especially at high temperatures, played by the insulating layers between the CuO_2 planes in flux pinning. Much stronger pinning centers need to be introduced into the tapes when the field is applied normal to the CuO_2 planes. Notice that, in both orientations, $J_{cm}(H)$ exhibits approximately the relation, $J_{cm}(H) \sim \exp(-H/H_0)$, which indicates that in the case of $H \perp c$, misalignment in the textured Bi-2223 tape leads to a field component parallel to the c-axis. J_{cm} for $H \parallel c$ is similar to $J_{ct}(H)$ as shown in Fig. 7, but $J_{cm}(H)$ has lower values which reflects different time constants or different voltage

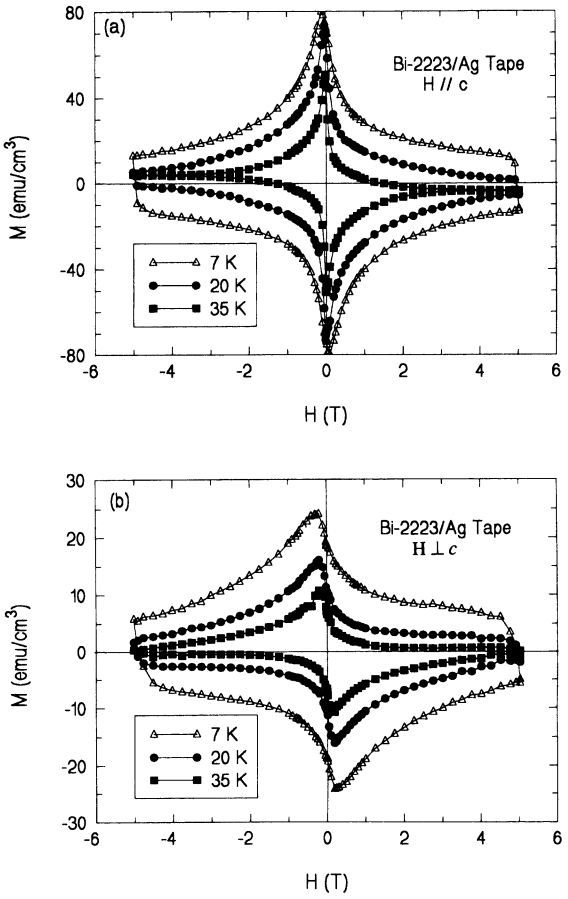

Fig. 8. Magnetic-hysteresis loops of a Ag sheathed Bi-2223 tape for (a) $H \parallel c$ and for (b) $H \perp c$.

sensitivity of the two measurements. The difference between J_{cm} and J_{ct} becomes more pronounced as the temperature is increased. It suggests that J_c at high temperatures is controlled by flux pinning, in contrast to intergranular junctions at low temperatures [5]. As compared with Bi-2212 single crystals, the less significant anisotropy of J_c observed in the Bi-2223 tapes can be attributed to the difference in the flux-penetration patterns in these materials. Taking into account the imperfect textured structure and possible stoichiometric variations at grain boundaries in our Bi-2223 tapes, here we likely obtain a result due to the contributions of multiple J_c components (i.e., parallel and perpendicular to the c-axis) that are difficult to separate.

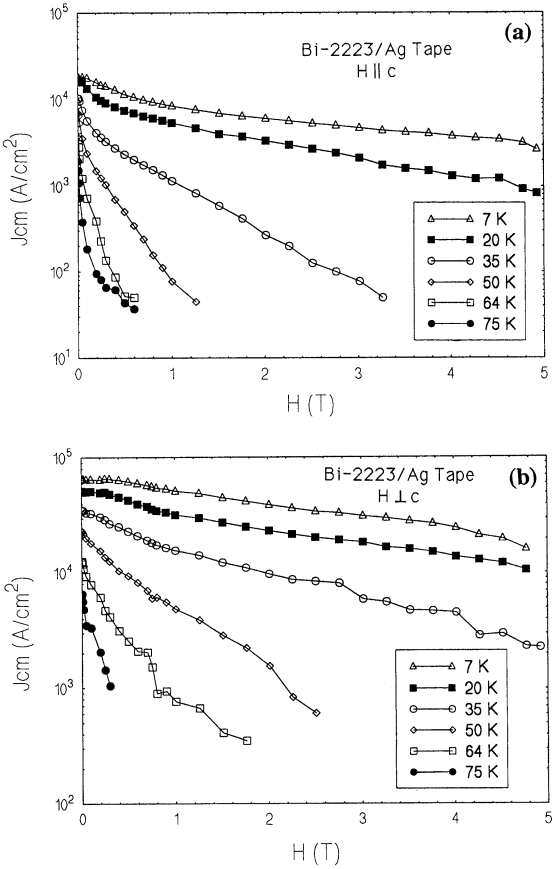

Fig. 9. Field dependence of J_{cm} in the cases of (a) $H \| c$ and (b) $H \perp c$.

3.5. 2D-like flux-creep behavior in Bi-2212 single crystals

As widely known, the widths of the magnetization loops change with the sweep rate of the magnetic field. This observation indicates that J_{cm}'s can significantly deviate from intrinsic J_c's due to flux creep. In this work, the decay of isothermal magnetization with time is therefore measured from the situation where the flux profile fully penetrates the sample for 10^4 s at constant magnetic field over a wide range of temperatures. The effective pinning energy, $U_{eff}(J)$, is calculated from the time derivative of the relaxation curves $M(t)$ as proposed by Maley et al. [37],

$$\frac{U_{eff}(J)}{k} = -T\left(\ln\left|\frac{dM}{dt}\right| - C\right), \qquad (3)$$

where $C = \ln(B\alpha\omega_0/(\pi d))$ is treated as a constant at low temperatures, ω_0 is a characteristic attempt frequency, α is a hop distance, and d is the sample thickness transverse to the applied field. C is determined to be the value that gives a smooth curve of U_{eff}/k versus J ($J \propto M$) in the low-temperature regime starting from the lowest measurement temperature, 5 K. Illustrated in Fig. 11 is a typical $U_{eff}(J)$ curve; the data recorded at temperatures above 8.5 K fall below the track extrapolated from the low-temperature data. To take into account this implicit temperature effect on U_{eff}, each set of isothermal data taken at $T > 8.5$ K is multiplied by a numerical value so that the data points measured at different temperatures fall on top of each other in the entire range of J [2,38]. A scaling function $G(T)$ that decreases with temperature is then extracted

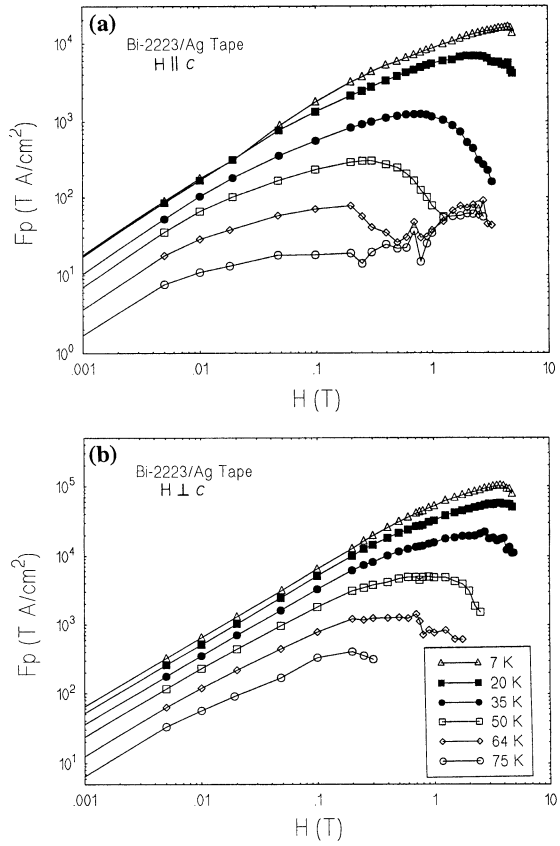

Fig. 10. Field dependence of the pinning-force density F_p in a Ag sheathed Bi-2223 tape for (a) $H \| c$ and (b) $H \perp c$.

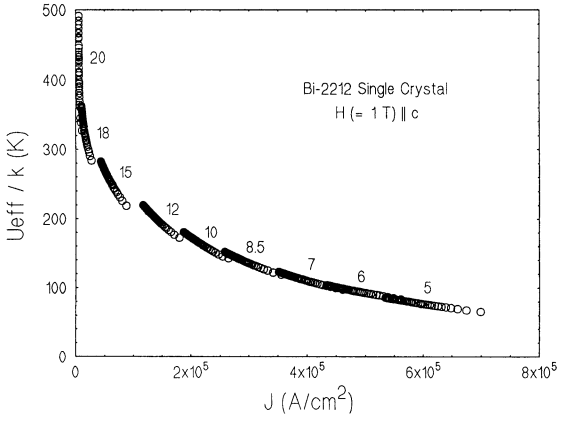

Fig. 11. $U_{\rm eff}/k$ vs. J for $H(=1\ {\rm T})\|c$ in a Bi-2212 single crystal.

from the inverse of these numerical values as will be described later. Fig. 12 shows $U_{\rm eff}(J)$ curves at 1 and 2 T after the implicit temperature dependence of $U_{\rm eff}$ is considered. These results are summarized:
(1) $U_{\rm eff}$ is a strongly nonlinear function of the current density. A weaker field dependence of $U_{\rm eff}$ is observed in $H\|c$ than in $H\perp c$. Because J's in these two orientations are different by two orders of magnitude, it is difficult to compare their $U_{\rm eff}$ values.
(2) The collective flux-pinning [39] and the vortex-glass [40] theories propose an inverse power-law expression for $U_{\rm eff}(J)$ as

$$U_{\rm eff}(J) \cong U_{\rm i}\left(\frac{J_{\rm i}}{J}\right)^{\mu}, \qquad (4)$$

where $U_{\rm i}$ is the scale of the activation energy, $J_{\rm i}$ is the current density, and the exponent μ is a value of order 1. $J_{\rm i}$ and μ both vary with the dimensionality of the vortex lattice and with the ratio of $J/J_{\rm c}$. For 3D flux creep, μ changes from $\frac{1}{7}$ to $\frac{3}{2}$ to $\frac{7}{9}$ as J decreases, accompanied by the variation in flux bundle sizes. In 2D systems, μ has the values of $\frac{9}{8}$ and $\frac{1}{2}$. Eq. (4) also implies that $U_{\rm eff}(J)$ diverges as the current density J approaches 0. For the case of $H\|c$, $U_{\rm eff}(J)$ increases gradually with decreasing current densities. The corresponding decreasing μ values are in good agreement with the 2D collective-creep theory. However, in the very low-J regime, the $U_{\rm eff}(J)$ curve levels off to a weak logarithmic increase rather than to diverge. This suggests that a transition to the plastic-creep regime possibly occurs. Such an effect is not incorporated in the elasticity-based vortex glass model [38,41]. In other words, the dislocation nucleation energy is much lower than the pinning energy and hence dominates the observed flux-creep characteristic. This then inhibits the existence of a vortex-glass state in 2D systems.

(3) In $H\perp c$, $U_{\rm eff}(J)$ curves can be approximately broken at around 10 K and 25 K into three distinct sections. As shown in Fig. 12(b) for a power-law form of $U_{\rm eff}(J)$, the experimental μ value for $T<10$ K and $T>20$ K is equal to 2.06. Its value decreases first and then increases with increasing temperatures as $T>10$ K. Similar examples of μ variations can also be found in the 3D Y-123 system,

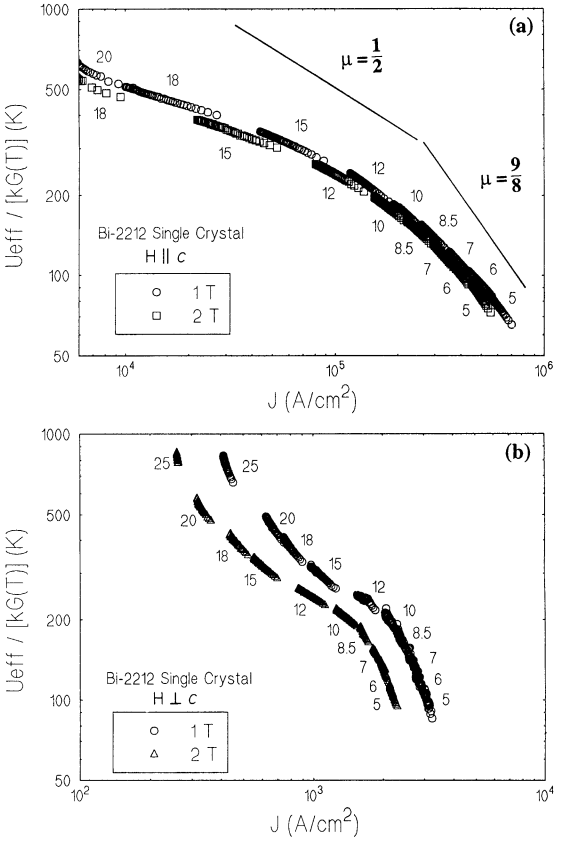

Fig. 12. A comparison of $U_{\rm eff}/kG(T)$ vs. J between (a) $H\|c$ and (b) $H\perp c$ in Bi-2212 single crystals. The numbers beside the curves represent the measurement temperatures. The solid lines are predicted from the collective flux creep theory for a 2D vortex lattice and drawn for comparison.

such as the dependence of μ on oxygen deficiencies in an aligned $YBa_2Cu_3O_{7+\delta}$ superconductor [42] and the effect of temperature on μ (from 1 to 3 with decreasing J in the low-J regime) in an ion-irradiated $YBa_2Cu_3O_7$ crystal [43]. These observations suggest the complexity of the interaction between vortex lattice and pinning centers. Nevertheless, different dissipation characteristics are clearly displayed here between $H \parallel c$ (see Fig. 5(a)) and $H \perp c$ (see Fig. 5(b)).

3.6. An anisotropy of effective pinning energies in Bi-2223 tapes

Magnetic relaxation in Ag sheathed Bi-2223 tapes was measured for $H \parallel c$ and $H \perp c$ at 1 and 2 T over 5–45 K. Although we had subtracted carefully the reversible magnetization from the measured M before we converted M to J, the relative small irreversible M values obtained at high temperatures inevitably posed some uncertainty in the low-J regime of the $U_{\text{eff}}(J)$ curves. More work is required to clarify this concern (see discussion in Section 3.7). Therefore, several isothermal data sets taken at low J are not shown in Fig. 13 that illustrates the $U_{\text{eff}}(J)$ curves after the implicit temperature dependence of $U_{\text{eff}}(J)$ is corrected. From the discussion in the previous section and the similarity in the anisotropic crystal structures between Bi-2212 and Bi-2223, we tend to believe that, in $H \parallel c$, $U_{\text{eff}}(J)$ is weakly J independent as $J \to 0$, which seems not to be the case in Fig. 13(a). However, as pointed out by Vinokur et al. [44] for small currents, a vortex-glass state may exist in a 2D system when $T < T_g = T_m/\ln(B/B_{2D})$, where T_m is the magnetic irreversibility temperature, and B_{2D} is the crossover field. Plastic creep, in general, takes place at some temperature $T_g < T < T_m$. Here, we may not record the data at temperatures high enough to be in the plastic-creep regime, or the situation is complicated by the percolative shielding current paths resulting from imperfect grain alignment. Nevertheless, several issues related to Fig. 13 are worthy to be mentioned:

(1) At a constant J, say, 9×10^3 A/cm^2, $U_{\text{eff}}(J)$ for $H \perp c$ is two orders of magnitude higher than that in $H \parallel c$. This reveals a much higher activation energy

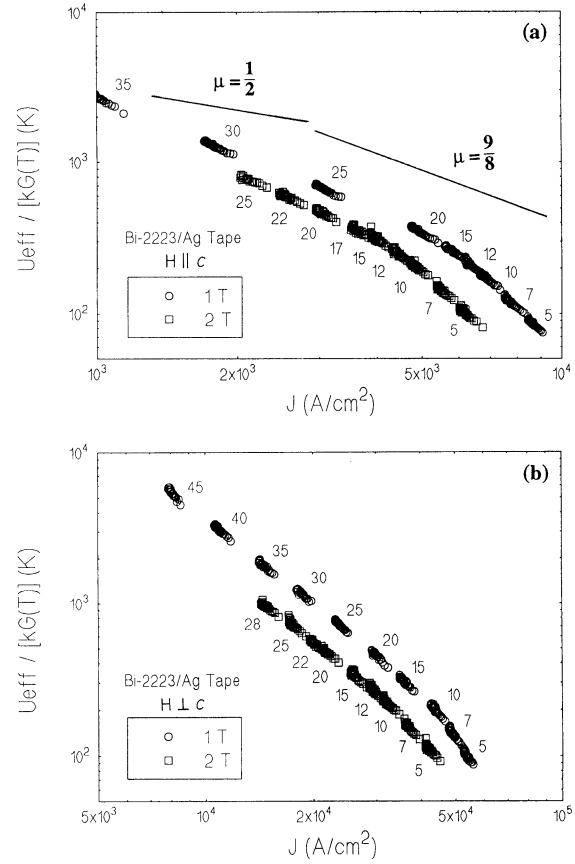

Fig. 13. The curves of $U_{\text{eff}}/kG(T)$ vs. J obtained for (a) $H \parallel c$ and (b) $H \perp c$ after the implicit temperature dependence of U_{eff} is corrected. The solid lines are drawn for comparison from the predictions of 2D collective flux creep. The numbers beside the curves represent the measurement temperatures. Notice that at a constant J, $U_{\text{eff}}(J)$ shows a higher value in $H \perp c$ than in $H \parallel c$.

associated with the intrinsic pinning mechanism in the case of $H \perp c$.

(2) In $H \parallel c$, the $U_{\text{eff}}(J)$ curves can be described well by the power-law dependence of J with two different μ values: $\mu = 2.95 \pm 0.02$ for $T < 20$ K at 1 T and $T < 15$ K at 2 T as well as $\mu = 1.20 \pm 0.08$ for the higher-temperature, low-J region of the data. The latter case appears to agree approximately with the 2D theoretical values of $\frac{9}{8}$. For $H \perp c$, except for the very low-temperature data, $U_{\text{eff}}(J)$ curves over a wide range of J exhibit $\mu = 1.87 \pm 0.03$.

(3) According to the rocking-curve measurement performed on our tapes, an average misalignment angle is estimated to be about $\pm 10°$. If Cho's obser-

vations [16] as mentioned earlier are correct, the imperfectly textured structure in the Bi-2223 tape can smear out the observed J dependence of U_{eff} to some extent. The likely percolative current flow in these polycrystalline tapes not only causes the difficulty in determining the exact J components (J_{ca}, J_{cb}, or J_{cc}) that are actually probed during the relaxation measurements, but also obscure a clear identification of the dimensionality of flux creep. In the case of $H \perp c$, the ratio of the dimension of the FLL unit cell to the spacing between the CuO_2 planes governs the presence of a 3D lattice or a 2D configuration of the Josephson junction in the samples. This, in turn, depends on the operating temperature and magnetic field, as well as the underlying pinning mechanisms. The interplay among the degree of texturing, pinning characteristics, and 2D/3D crossover in the tapes likely needs to be further investigated before drawing a conclusion concerning the $U_{\text{eff}}(J)$ curves.

3.7. A comparison of Bi-2212 single crystals with Bi-2223 tapes

Bi-2212 and Bi-2223 have a similar layered structure and the main difference between these two superconductors is the number of the adjacent Cu–O planes in their crystals. This causes different T_c's, i.e., 85 K versus 110 K. In principle, if they are perfect single-crystal material, they should exhibit the similar electrical and magnetic behavior. However, in this work, they are prepared by different methods: one is a single crystal and the other is polycrystalline. The degree of texturing, intergranular coupling, and the nature and density of defects are different and expected to influence their properties. One can also view this as a way to study how these factors affect their flux-creep characteristics. For this purpose, we first calculate the normalized relaxation rate, $S = -\mathrm{d}M/M_0 \mathrm{d}\ \ln\ t \cong -\mathrm{d}\ \ln\ M/\mathrm{d}\ \ln\ t$, and plot it in Fig. 14, where M_0 is the initial magnetization. The Bi-2212 single crystal obviously has much higher S values than those obtained in the Bi-2223 tape. The former exhibits a maximum in each field and orientation, whereas the latter show multiple local maxima in the $S(T)$ curves. The S values for Bi-2223 tapes are close to what were

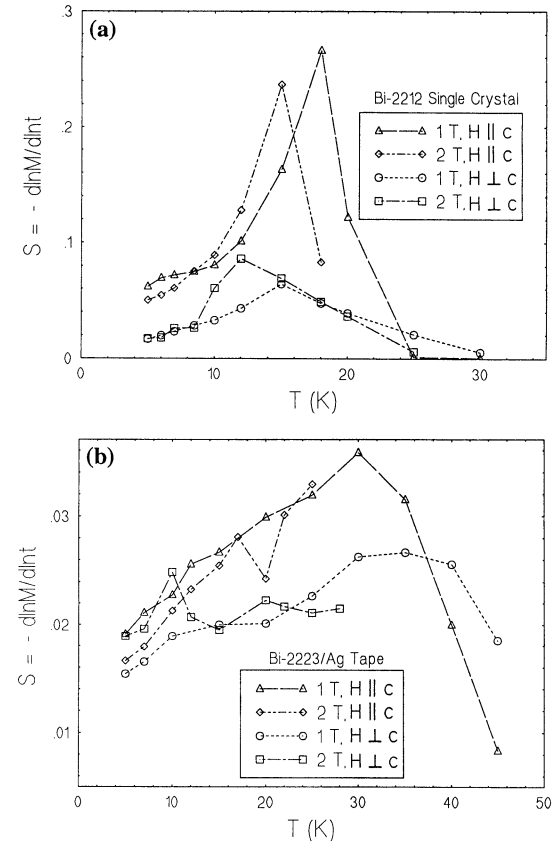

Fig. 14. The temperature dependence of the normalized relaxation rate, $S(T)$, at 1 and 2 T for (a) Bi-2212 single crystals and (b) Bi-2223 tapes.

obtained by Mittag et al. [45]. As illustrated in Fig. 14, the $S(T)$ maximum shifts towards lower temperatures with increasing magnetic field, and at the same field, it seems to occur at a lower temperature in $H \perp c$ than in $H \parallel c$. Notice that in Bi-2212 single crystals, the position of the maximum is near the temperature where a dramatic change in the slope of $U_{\text{eff}}(J)$ curve takes place. Besides, a significant anisotropy in $S(T)$ exists between $H \parallel c$ and $H \perp c$, which is opposite to Umemura's observations [46]. The magnitude of the maximum in $H \parallel c$ is much higher as compared with the entire $S(T)$ curve, and this corresponds to a transition into the plastic-creep regime. In contrast to this behavior, imperfect texturing and the presence of grain boundaries in the Bi-2223 tapes probably cause their S values to show a weaker temperature dependence. These results,

Table 1
The parameters for curve fitting $U_{eff}(J, T, H) = U_i/H^n[1-(T/T_x)^2]^{1.5}(J_i/J)^\mu$ in the Bi-2212 single crystals

Case	C	T_{irr} (K)	T_x (K)	n	μ
$H \parallel c$	13 (1 T)	45.0 (1 T)			
($F_L \parallel ab$)			43.0	0.11	1.13 ($T \leq 8.5$ K) and 0.50 ($T > 8.5$ K)
	14 (2 T)	34.5 (2 T)			
$H \perp c$	12 (1 T)	60.0 (1 T)			
($F_L \parallel ab$)			55.0	varying	2.06 ($T < 10$ K and $T > 20$ K) and varying (10 K $\leq T \leq$ 20 K)
	14 (2 T)	52.0 (2 T)			

indeed, do not completely support the previously suggested plateau-like dependence of $S(T)$ [47].

Referring to Fig. 6 and Fig. 10, for $H \parallel c$ at low temperatures, pinning force density F_p, which is oriented along the ab plane, is higher in Bi-2212 single crystals than in Bi-2223 tapes. However, this difference becomes less significant with increasing temperatures, for instance, compare the data at $T = 0.35T_c$. Because we observe a more homogeneous distribution of dislocation networks and unidentified precipitates in the Bi-2223 tape, the above result could be indicative of the effect of thermomechanical process on the flux creep. In the case of $H \perp c$, both systems are of the same order of magnitude in F_p, but Bi-2223 tapes show the weaker temperature dependence of F_p. This probably results from a measurement probing the intrinsic pinning force parallel to the c-axis in the Bi-2223 tape versus an F_p perpendicular to the c-axis of the Bi-2212 single crystal.

As described earlier, the scaling function, $G(T)$, is introduced to correct the implicit temperature dependence of $U_{eff}(J)$. The results reveal that $U_{eff}(J)$ is less temperature dependent in $H \perp c$ than in $H \parallel c$. The empirical expression for $G(T)$ at all data can be very well fit to the relation $G(T) = [1-(T/T_x)^2]^{1.5}$. Here, $T_x = 43$ K ($H \parallel c$) and 55 K ($H \perp c$) for Bi-2212, and 49 K ($H \parallel c$) and 59.5 K ($H \perp c$) for Bi-2223. These values are not exactly equal to the corresponding magnetic irreversibility temperatures, T_{irr}'s, as listed in Tables 1 and 2. But, T_x can be qualitatively related to T_{irr}. This is a great contrast to the temperature dependence established for Y-123 [2], where it was shown that $T_x \sim T_{irr} \sim T_c$. The fact that $T_x \ll T_c$ for the Bi based materials indicates the pinning/activation energies are vanishing at temperatures much below T_c. This may be seen as evidence for vortex-lattice melting or thermally driven decoupling between the CuO_2 layers.

We have also investigated the field scaling H^{-n} of $U_{eff}(J)$ so that the curves at different fields coincide. In Bi-2212 single crystals, $n = 0.11 \pm 0.01$ is found appropriate for $H \parallel c$, but it varies between 0.26 and 0.89 for $H \perp c$. In Bi-2223 tapes, a single value, $n = 0.78 \pm 0.02$, can describe all the temperatures we measured for $H \parallel c$. However, two values of n are needed for the case of $H \perp c$, namely, $n = 1.00 \pm 0.01$ and 0.50 ± 0.03 for $T < 15$ K and $T \geq 15$ K, respectively. Roughly speaking, in both superconductors, n values for the field dependence of U_{eff} are of the order of 1.0. The relation $U \approx B^{-1/2}$ was previously observed in the Ag sheathed Bi-2212 wires from the Arrhenius plot of f (Hz) versus $1/T_{irr}$ (K^{-1}) determined by AC susceptibility in the fre-

Table 2
The parameters for curve fitting $U_{eff}(J, T, H) = U_i/H^n[1-(T/T_x)^2]^{1.5}(J_i/J)^\mu$ in the Ag sheathed Bi-2223 tapes

Case	C	T_{irr} (K)	T_x (K)	n	μ
$H \parallel c$	9 (1 T)	50.0 (1 T)			
($F_L \parallel ab$)			49.0	1.00 ($T < 15$ K) and 0.50 ($T > 15$ K)	2.95 ($T \leq 15$ K) and 1.20 ($T > 15$ K)
	12 (2 T)	47.5 (2 T)			
$H \perp c$	11 (1 T)	65.0 (1 T)			
($F_L \parallel c$)			59.5	0.78	4.85 ($T \leq 10$ K) and 1.87 ($T > 10$ K)
	13 (2 T)	58.0 (2 T)			

quency range 500–100 000 Hz [10]. Another example for the field dependence of U obtained from the $\rho = \rho_0 \exp(-U/T)$ measurement of Bi-2212 single crystals was given as $U \sim H^{-n}$ with $n = \frac{1}{2}$ ($H < 1$ T) and $\frac{1}{6}$ ($H > 1$ T) in the case of $H \perp c$, and $\frac{1}{6}$ ($H < 3$ T) and $\frac{1}{3}$ ($H > 3$ T) in the case of $H \parallel c$ [48]. The slight discrepancy among these results can be attributed to the different sensitivity associated with the measurement techniques and the sample quality. The final expression for the effective pinning energy U_{eff} is thus written as

$$U_{\text{eff}}(J,T,H) = \frac{U_i}{H^n}\left[1 - \left(\frac{T}{T_x}\right)^2\right]^{1.5}\left(\frac{J_i}{J}\right)^{\mu}. \qquad (5)$$

The results are also summarized in Tables 1 and 2. Based on Eq. (5), the $U_{\text{eff}}(J)$ behavior in both Bi-2212 single crystals and Bi-2223 tapes can be described by a power-law relation. If we take the dimensional crossover field $B_{2D} = 65$ mT for $H \parallel c$ in Bi-2212 single crystal [49] and $T_m = T_{irr} = 45$ K and 34.5 K at 1 T and 2 T, respectively, as we measured, we will obtain the corresponding T_g values as 16.5 K and 10 K. At temperatures above T_g (see Section 3.6), the power law is broken down and the plastic-creep mechanism begins to dominate. A weaker dependence of U_{eff} on J should be observed. This is exactly the result depicted in Fig. 12(a). In the case of Bi-2223 tapes, we have not been able to probe this situation. We are limited by the method employed in this work to analyze relaxation data and the lack of locally perfect-aligned Bi-2223 samples with clean grain boundaries. An approach to separating the effect of the current density from temperature on U_{eff} should be developed. In Fig. 13(a), we may be in the regime still far below T_g. For the $H \perp c$ orientation, we believe that we obtained a net effect due to in-plane and out-of-plane shielding currents. The predominant one depends strongly on temperature, field, and even on local geometry and stoichiometry [50].

4. Conclusions

The difference in hysteretic response, critical current density, and flux pinning in the Bi based superconductors, in relation to field orientations, can be attributed to different interactions between the supercurrent and the intrinsically pinned ($H \perp c$) and pancake ($H \parallel c$) vortices. In bulk samples, when material texturing is not completely achieved (e.g., our Ag sheathed Bi-2223 tapes), these two effects may not be clearly distinguished; for instance, a field component parallel to the c-axis, which gives rise to dissipative behavior and controls J_c, can exist even when the magnetic field is applied perpendicular to the c-axis. In the present work, $Bi_2Sr_2CaCu_2O_{8+\delta}$ (Bi-2212) single crystals and Ag sheathed $(Bi,Pb)_2Sr_2Ca_2Cu_3O_{10+\delta}$ (Bi-2223) tapes have been characterized by magnetometry and electron microscopy. In Bi-2212 single crystals studied here, because of their aspect ratios, for both cases of $H \parallel c$ and $H \perp c$, the measurable Lorentz forces (F_L) that limit J_c are found to be perpendicular to the c-axis; one causing vortices to hop in the ab plane and the other to slide along the ab plane. In Bi-2223 tapes, on the other hand, the relative strength ratio of the intrinsic pinning to the extrinsic pinning has been probed. For the same average J value, the effective pinning energy (U_{eff}) calculated from the time derivative of magnetization (M) for $H \perp c$ is two orders of magnitude higher than that in $H \parallel c$. For these two superconductors, their U_{eff}'s follow a power-law expression, $U_{\text{eff}}(J, T, H) = (U_i/H^n)[1 - (T/T_x)^2]^{1.5}(J_i/J)^{\mu}$, where $0.11 \le n \le 1.00$ and $0.5 \le \mu \le 4.85$. A two-dimensional (2D) flux-line lattice (FLL) is clearly identified in the Bi-2212 single crystal; however, small misalignments in the Bi-2223 tape add uncertainty to the information on the dimensionality that can be deduced from the U_{eff} (J) curves. Much higher values of normalized relaxation rate, $S = -\mathrm{d}\ln M/\mathrm{d}\ln t$ are observed in Bi-2212 than Bi-2223.

Acknowledgement

This work was supported by the United States Department of Energy, Office of Energy Management.

References

[1] M. Murakami, M. Morita, K. Doi and M. Miyamoto, Jpn. J. Appl. Phys. 28 (1989) 1189.

[2] P.J. Kung, M.P. Maley, M.E. McHenry, J.O. Willis, M. Murakami and S. Tanaka, Phys. Rev. B 48 (1993) 13922.
[3] L.J. Swartzendruber, D.L. Kaiser, F.W. Gayle, L.H. Bennett and A. Roytburd, Appl. Phys. Lett. 58 (1991) 1566.
[4] Y. Feng, K.E. Hautanen, Y.E. High, D.C. Larbalestier, R. Ray II, E.E. Hellstrom and S.E. Babcock, Physica C 192 (1992) 293.
[5] H.K. Liu, Y.C. Guo, S.X. Dou, S.M. Cassidy, L.F. Cohen, G.K. Perkins, A.D. Caplin and N. Savvides, Physica C 213 (1993) 95.
[6] Q.Y. Hu, H.W. Weber, S.X. Dou, H.K. Liu and H.W. Neumüller, J. Alloys Comp. 195 (1993) 515.
[7] P. Schmitt, P. Kummeth, L. Schultz and G. Saemann-Ischenko, Phys. Rev. Lett. 67 (1991) 267.
[8] J.R. Clem, Phys. Rev. B 43 (1991) 7837.
[9] M. Tachiki and S. Takahashi, Solid State Commun. 70 (1989) 291.
[10] K. Heine, J. Tenbrink and M. Thoner, Appl. Phys. Lett. 55 (1989) 2441.
[11] K. Sato, T. Mikata, H. Mukai, M. Ueyama, T. Kato, T. Masuda, M. Nagata, K. Iwata and T. Misui, IEEE Trans. Magn. 27 (1991) 1231.
[12] J.E. Tkaczyk, R.H. Arendt, M.F. Garbauskas, H.R. Hart, K.W. Lay and F.E. Luborsky, Phys. Rev. B 45 (1992) 12506.
[13] L.N. Bulaevskii, J.R. Clem, L.I. Glazman and A.P. Malozemoff, Phys. Rev. B 45 (1992) 2545.
[14] A. Umezawa, Y. Feng, H.S. Edelman, Y.E. High, D.C. Larbalestier, Y.S. Sung, E.E. Hellstrom and S. Fleshler, Physica C 198 (1992) 261.
[15] B. Hensel, J.-C. Grivel, A. Jeremie, A. Perin, A. Pollini and R. Flükiger, Physica C 205 (1993) 329.
[16] J.H. Cho, M.P. Maley, J.O. Willis, J.Y. Coulter, L.N. Bulaevskii, P. Haldar and L.R. Motowidlo, Appl. Phys. Lett. 64 (1994) 3030.
[17] M.J.V. Menken, A.J.M. Winkelman and A.A. Menovsky, J. Cryst. Growth 113 (1991) 9.
[18] S.A. Sunshine, T. Siegrist, L.F. Schneemeyer, D.W. Murphy, R.J. Cava, B. Batlogg, R.B. van Dover, R.M. Fleming, S.H. Glarum, S. Nakahara, R. Farrow, J.J. Krajewski, S.M. Zahurak, J.W. Wasczak, J.H. Marshall, P. Marsh, L.W. Rupp Jr. and W.F. Peck, Phys. Rev. B 38 (1988) 893.
[19] R. Mokrani, M. Ben Salem, O. Monnereau, F. Remy, G. Vacquier and C. Boulesteix, Rev. Phys. Appl. 25 (1990) 45.
[20] E. Takayama-Muromachi, Y. Uchida, A. Ono, F. Izumi, M. Onoda, Y. Matsui, K. Kosuda, S. Takekawa and K. Kato, Jpn. J. Appl. Phys. 27 (1988) L365.
[21] C.H. Chen, D.J. Werder, S.H. Liou, H.S. Chen and M. Hong, Phys. Rev. B 37 (1988) 9834.
[22] P.H. Kes and C.J. van der Beek, Mater. Res. Soc. Symp. Proc., Vol. 275 (Mater. Res. Soc., Pittsburgh, 1992) p. 157.
[23] O. Eibl, Physica C 168 (1990) 239.
[24] G. Yang, S. Sutton, P. Shang, C.E. Gough and J.S. Abell, IEEE Trans. Appl. Supercond. 3 (1993) 1663.
[25] R. Ramesh, B.G. Bagley, J.M. Tarascon, S.M. Green, M.L. Rudee and H.L. Luo, J. Appl. Phys. 67 (1990) 379.
[26] S.X. Dou, H.K. Liu, J. Wang and W.M. Bian, Supercond. Sci. Technol. 4 (1991) 21.
[27] C.P. Bean, Phys. Rev. Lett. 8 (1962) 250.
[28] A. Umezawa, G.W. Crabtree, J.Z. Liu, W. Weber, W.K. Kwok, L.H. Nunez, T.J. Moran, C.H. Sowers and H. Claus, Phys. Rev. B 36 (1987) 7151.
[29] S. Martin, F.T. Fiory, R.M. Fleming, G.P. Espinosa and A.S. Cooper, Appl. Phys. Lett. 54 (1989) 72.
[30] B.D. Biggs, M.N. Kunchur, J.J. Lin, S.J. Poon, T.R. Askew, R.B. Flippen, M.A. Subramanian, J. Gopalakrishnan and A.W. Sleight, Phys. Rev. B 39 (1989) 7309.
[31] S. Nomura, Y. Yamada, T. Yamashita and H. Yoshino, J. Appl. Phys. 67 (1990) 547.
[32] M.P. Maley, P.J. Kung, J.Y. Coulter, W.L. Carter, G.N. Riley and M.E. McHenry, Phys. Rev. B 45 (1992) 7566.
[33] H.-W. Neumüller, W. Gerhäuser, G. Ries, P. Kummeth, W. Schmidt, S. Klaumünzer and G. Saemann-Ischenko, Cryogenics 33 (1993) 14.
[34] M.E. McHenry, P.J. Kung, M.P. Maley, J.O. Willis and J.Y. Coulter, IEEE Trans. Appl. Supercond. 3 (1993) 1143.
[35] P.J. Kung, M.P. Maley, P.G. Wahlbeck and D.E. Peterson, J. Mater. Res. 8 (1993) 713.
[36] J.-I. Kase, K. Togano, H. Kumakura, D.R. Dietderich, N. Irisawa, T. Morimoto and H. Maeda, Jpn. J. Appl. Phys. 29 (1990) L1096.
[37] M.P. Maley, J.O. Willis, H. Lessure and M.E. McHenry, Phys. Rev. B 42 (1990) 2639.
[38] C.J. van der Beek, P.H. Kes, M.P. Maley, M.J.V. Menken and A.A. Menovsky, Physica C 195 (1992) 307.
[39] M.V. Feigel'man, V.B. Geshkenbein and V.M. Vinokur, Phys. Rev. B 43 (1991) 6263.
[40] M.P.A. Fisher, Phys. Rev. Lett. 62 (1989) 1415.
[41] C.J. van der Beek and P.H. Kes, Phys. Rev. B 43 (1991) 13032.
[42] J.G. Ossandon, J.R. Thompson, D.K. Christen, B.C. Sales, Y. Sun and K.W. Lay, Phys. Rev. B 46 (1992) 3050.
[43] M. Konczykowski, V.M. Vinokur, F. Rullier-Albenque, Y. Yeshurun and F. Holtzberg, Phys. Rev. B 47 (1993) 5531.
[44] V.M. Vinokur, P.H. Kes and A.E. Koshelev, Physica C 168 (1990) 29.
[45] M. Mittag, R. Job and M. Rosenberg, Physica C 174 (1991) 101.
[46] T. Umemura, K. Egawa, S.-I. Kinouchi, J. Tanimura, A. Nozaki and S. Utsunomiya, J. Appl. Phys. 71 (1992) 2765.
[47] A.P. Malozemoff and M.P.A. Fisher, Phys. Rev. B 42 (1990) 6784.
[48] T.T.M. Palstra, B. Batlogg, L.F. Schneemeyer and J.V. Waszczak, Phys. Rev. Lett. 61 (1988) 1662.
[49] R. Cubitt, E.M. Forgan, G. Yang, S.L. Lee, D.McK. Paul, H.A. Mook, M. Yethiraj, P.H. Kes, T.W. Li, A.A. Menovsky, Z. Tarnawski and K. Mortensen, Nature (London) 365 (1993) 407.
[50] D.C. Larbalestier, X.Y. Cai, Y. Feng, H. Edelman, A. Umezawa, G.N. Riley Jr. and W.L. Carter, Physica C 221 (1994) 299.